frontiers in Physics

REVIEW
published: 17 December 2020
doi: 10.3389/fphy.2020.598420

Coherent Anti-Stokes Raman Scattering Microscopy and Its Applications

*Shaowei Li, Yanping Li, Rongxing Yi, Liwei Liu and Junle Qu**

College of Physics and Optoelectronic Engineering, Shenzhen University, Shenzhen, China

Coherent anti-Stokes Raman scattering (CARS) microscopy can provide high resolution, high speed, high sensitivity, and non-invasive imaging of specific biomolecules without labeling. In this review, we first introduce the principle of CARS microscopy, and then discuss its configuration, including that of the laser source and the multiplex CARS system. Finally, we introduce the applications of CARS in biomedicine and materials, and its future prospects.

Keywords: Raman scattering, coherent anti-Stokes Raman scattering, nonlinear optical microscopy, label-free imaging, biomedical imaging

OPEN ACCESS

Edited by:
Ming Lei,
Xi'an Jiaotong University, China

Reviewed by:
Kebin Shi,
Peking University, China
Ping Wang,
Huazhong University of Science and Technology, China

****Correspondence:***
Junle Qu
jlqu@szu.edu.cn

Specialty section:
This article was submitted to Optics and Photonics, a section of the journal Frontiers in Physics

Received: *24 August 2020*
Accepted: *06 October 2020*
Published: *17 December 2020*

Citation:
Li S, Li Y, Yi R, Liu L and Qu J (2020) Coherent Anti-Stokes Raman Scattering Microscopy and Its Applications. Front. Phys. 8:598420. doi: 10.3389/fphy.2020.598420

INTRODUCTION

Raman scattering was named after its discoverer C. V. Raman, the celebrated Indian scientist, in 1928 [1]. The discovery of Raman scattering not only proved that the energy level of light is discrete but also opened up a new research area for the study of the chemical characteristics of molecules. First, Raman scattered photons in the mid-infrared range carry information about molecular vibration. The switch from infrared to visible light circumvents the strong optical absorption of water in the infrared region, which is of great significance in the field of biomedical science. Second, Raman spectroscopy obviates the need for chemical labeling when obtaining chemical information, so that the biological functional characteristics of the sample can be studied without chemical interference.

Although it has many advantages, spontaneous Raman scattering is a very weak second-order radiative process. The cross-section of Raman scattering is approximately 10–30 cm^2 per molecule, which is 10^{11} times smaller than the corresponding cross-section of infrared absorption. The small cross-section of the scattering leads to a low spontaneous Raman scattering efficiency and consequently necessitates a long integration time. This is acceptable for Raman spectroscopy, but for imaging, it is not feasible to collect real-time data with such a long integration time. The development of the femtosecond laser with high peak power has enabled the observation of many nonlinear processes, and promoted the study of coherent Raman scattering.

As a new nonlinear optical microscopy technique, coherent Raman scattering microscopy overcomes the limitation of the imaging speed of spontaneous Raman micro-imaging [2–8]. In coherent Raman scattering microscopy, typically, two beams of light are used to simultaneously excite the sample, one beam is referred to as the pump beam and the other is the Stokes beam. When the frequency difference between the two beams of light corresponds to a chemical bond vibrational frequency of the target sample, four simultaneous coherent Raman processes will occur. These processes are coherent anti-Stokes Raman scattering at the frequency $(\omega_p - \omega_s) + \omega_p$, coherent Stokes Raman scattering at the frequency $\omega_p - (\omega_p - \omega_s)$, stimulated Raman gain at ω_s, and stimulated Raman loss at ω_p. The CARS signal is generated at a frequency that is different from the excitation light. Stimulated Raman gain and stimulated Raman loss are both employed in another

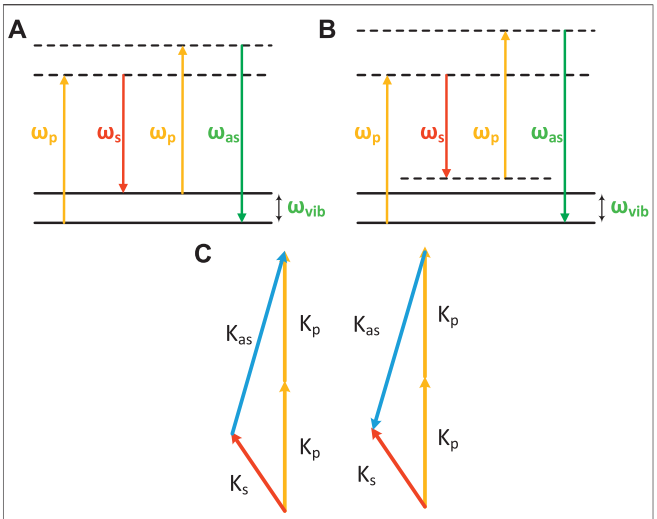

FIGURE 1 | Energy diagrams of the CARS process. Energy diagram of the **(A)** resonant condition and **(B)** non-resonant condition. **(C)** Phase-matching condition of CARS.

coherent Raman microscopy technique referred to as Stimulated Raman Scattering (SRS) Microscopy.

The first observation of CARS was reported by Terhune and Maker [9], as a third-order nonlinear effect in 1965 at Ford Motor Company, the car manufacturer. However, the official name of CARS was not coined until 10 years later by Begley [10]. Begley and his co-workers used CARS to study the chemical reaction kinetics of combustion. CARS microscopy was first implemented by Duncan [11] in 1982 using a non-collinear geometry to match the phase and obtain two-dimensional images. In 1999, Zumbusch [12] changed the excitation light configuration to overlap collinearly with the Stokes beam, and used a femtosecond laser for close focusing to achieve fast three-dimensional imaging. This work greatly promoted the rapid development of modern CARS microscopy technologies. Over the next few years, a systematic study of CARS was performed by Cheng and co-workers [2, 13–16]. In 2001, Cheng exploited polarization-CARS by using the difference between the polarizations of resonant and non-resonant CARS signals to eliminate the non-resonant background. Laser scanning CARS microscopy based on the picosecond pulsed laser was developed for high-speed imaging of biomedical samples [16], and the imaging speed of CARS reached the level of video-rate (20 frames/s) in 2005 [17]. Many strategies, including frequency modulation [18], nonlinear interferometric vibrational imaging [19], and spectral mixing [20] were used to suppress the non-resonant background or extract the pure Raman responses from the CARS spectrum.

In this review, the history and early development of CARS are introduced, as well as the implementation of both single frequency and multiplex CARS. Subsequently, recent applications in biomedical and material science are presented. Finally, the future directions of CARS are discussed.

CARS PRINCIPLE

CARS is a third-order nonlinear optical process. Under the interaction of $E(p)$, $E(s)$ of the Stokes light field and $E'(p)$ of the probe light field, the sample molecules will produce an anti-Stokes field E (as) with a frequency of $\omega_{as} = 2\omega_p - \omega_s$. **Figure 1** shows the energy diagram of the CARS process. **Figures 1A,B** show the generation process of the resonant CARS and non-resonant CARS signals, respectively, under the action of the pump light. In most cases, both the pump and probe light originate from the same laser beam; thus, in the above process, I_{CARS} describes the intensity of the CARS signal and is given by

$$I_{\mathrm{CARS}} \propto \left|\chi^{(3)}\right|^{(2)} I_p^2 I_s \left|\frac{\sin(\Delta kz/2)}{\Delta \mathrm{k}/2}\right|^2 \tag{1}$$

Where $k_i = 2\pi/\lambda_i$ is the wavevector, z is the thickness of the sample, and the wavevector mismatch Δk is defined as $\Delta k = k_{as} - (2K_p - k_s)$. When Δk z is close to zero, the sinc function is maximized. This condition is known as the phase-matched condition. **Figures 1C** exhibits the phase-matched conditions for forward- and epi-detected CARS signals. Here $\chi^{(3)}$ is the third-order polarizability which is usually expressed in the following form:

$$\chi^{(3)} = \chi_{NR}^{(3)} + \frac{\chi_R^{(3)}}{\Delta - i\Gamma} \tag{2}$$

where Δ is the Raman shift, which can be described as $\Delta = \omega_p - \omega_s - \Omega_R$, and Ω_R is the center frequency of a Raman line with bandwidth Γ. Hence, the CARS signal can be written as

$$I_{CARS} \propto \left|\chi_{NR}^{(3)}\right|^2 + \left|\chi_R^{(3)}(\Delta)\right|^2 + 2\chi_{NR}^{(3)} Re\chi_R^{(3)}(\Delta) \tag{3}$$

As can be seen from **Eq. 3**, the CARS intensity is determined by three terms: the first term is known as the non-resonant

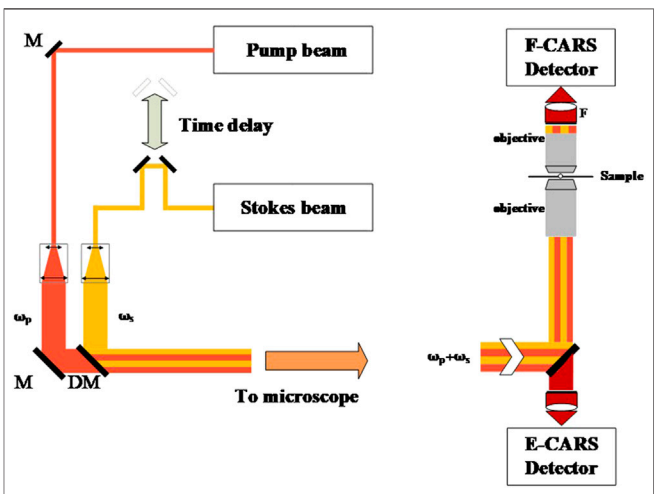

FIGURE 2 | (A) Spatio-temporal combination of pump and Stokes beams. **(B)** CARS signal collection: forward-CARS (F-CARS) and backward (epi)-CARS (E-CARS).

background and is independent of the Raman shift. The second term is the dominant contribution to probing strong resonant scatterers. The third term includes a mixture of resonant and non-resonant contributions, which contains the real part of the vibrational response.

CARS MICROSCOPY

Two pulsed laser trains at different frequencies, i.e., ω_p and ω_s, are necessary to build a CARS microscope (**Figure 2A**). One beam of the lasers is tunable to adjust the desired Raman shift, $\omega_p - \omega_s$. A pair of mirrors on a motorized linear stage is used to adjust the time delay between the pump and Stokes beams. Expanded beams are combined in a collinear geometry, and then directed to an inverted or upright microscope. Finally, the two temporally and spatially overlapped beams are focused onto the sample using a water/oil immersion objective lens. The strong CARS signals are generated both in the forward and backward direction, and are referred to as F-CARS and E-CARS, respectively (**Figure 2B**). Each signal is collected by a photomultiplier tube (PMT) or an avalanche photodiode after filtering the useless fluorescence with a bandpass filter, and focused by a lens. CARS images are obtained by a laser scanning system similar to that of a laser scanning confocal fluorescence microscope.

The cost and complexity of coherent Raman microscopy are mainly due to the laser light source. The two excitation beams must accurately control the absolute wavelength and linewidth. Although a pulsed dye laser in the visible band was used in the first coherent Raman microscopy system in history [11], the current mainstream light source for CARS is the Ti: sapphire laser or optical parametric oscillator (OPO) [17, 21]. Although the newly developed fiber laser-based coherent Raman microscopy can greatly reduce cost, it still cannot surpass solid-state lasers in performance [22, 23].

At least two excitation light sources are required for coherent Raman microscopy, one of which must be tunable to match the Raman frequency difference of different molecular vibration frequencies. For laser pulse width, a balance must be established; femtosecond has a shorter pulse width, higher peak power, and stronger nonlinear effect, while picosecond laser has narrower linewidth (l–10 cm^{-1} for a similar molecular vibration width) and can excite coherent Raman scattering more efficiently. Experiments show that pulses of 1–10 picoseconds can ideally achieve this balance [24]. For high-speed imaging, a repetition rate of at least 10 MHz is required, and ideally a higher rate. In addition, the laser excitation of the spectrum in the near infrared region can minimize the generation of the non-resonant background in CARS [12], providing less light-induced damage than visible light, and deeper penetration into the tissue. Further, because near-infrared light has a low transmission efficiency in a coherent Raman microscopy system (typically 10%–20% from excitation light to the sample), the power of the excitation source is approximately at the milliwatt level. Several groups have reported that they employed 50–200 fs pulse widths rather than a 2–6 picosecond pulse width [22, 25–27]. In spite of the fact that coherent Raman scattering processes could be excited by femtosecond pulses, this resulted in decreased signal levels, broader spectral resolution, and higher intensity non-resonant background signals.

CARS microscopy offers many unique advantages, including 1) nondestructive molecular imaging without labeling, 2) ease of spectral separation from the single-photon fluorescence background, and 3) 3D sectioning capability. Despite all of its advantages, however, the non-resonant background that limits the sensitivity of CARS is a major disadvantage.

MULTICOLOR CARS MICROSCOPY

Multicolor CARS microscopy refers to a method that can detect all or part of the vibration spectrum information on a sample at the same time. Multicolor CARS microscopy can be understood as a technique that can acquire a certain vibration spectrum such as a spontaneous Raman spectrum, but which has good imaging speed and spatial resolution. Although the imaging speed of multicolor CARS microscopy is still not as fast as that of single-color CARS, it has two essential advantages. The first is that multi-color CARS can obtain a full range of spectral information, while single-color can only obtain information at a certain frequency. The second is that multicolor CARS can better achieve quantitative analysis. Most microscopy techniques endeavor to achieve qualitative analysis at a certain point of the sample; however, in the fields of biology and material science, quantitative analysis of the composition of the sample is often required.

There are several common methods of implementing multicolor CARS microscopy, as shown in **Figure 3**. **Figures 3A** shows multicolor CARS microscopy using picosecond pump and femtosecond Stokes pulses [28, 29], in which a 100-fs Stokes pulse is used to provide a frequency domain window of approximately 400 cm^{-1}, which is sufficient to obtain the spectrum of the entire CH stretching range. In addition, by adjusting the center wavelength of the Stokes pulse, other regions of the vibration spectrum can also be studied, although not simultaneously. Using a 10-ps pump pulse can achieve a high spectral resolution of 2–3 cm^{-1}. **Figures 3B** shows multicolor CARS microscopy using picosecond pump and supercontinuum Stokes pulse [30–37]. Although a femtosecond Stokes pulse can include 400 cm^{-1} of spectral information in one-shot, this is still not sufficient for a vibrational frequency domain of 4,000 cm^{-1}. With the rapid development of photonic crystal fiber-based supercontinuum light sources, it has become feasible to use supercontinuum light sources as Stokes sources for CARS microscopy and to achieve a window of 4,000 cm^{-1}. Femtosecond and nanosecond sources are used to generate the supercontinuum spectrum. **Figures 3C** shows multicolor CARS using a femtosecond pump and Stokes pulse with spectral focusing [30, 38–44], and **Figures 3D** shows the principle of the spectral focusing method. In general, by using broadband pump and broadband Stokes pulses, the spectral resolution of the CARS signal is reduced. Hellerer [38] proposed the method of spectral focusing in 2004,

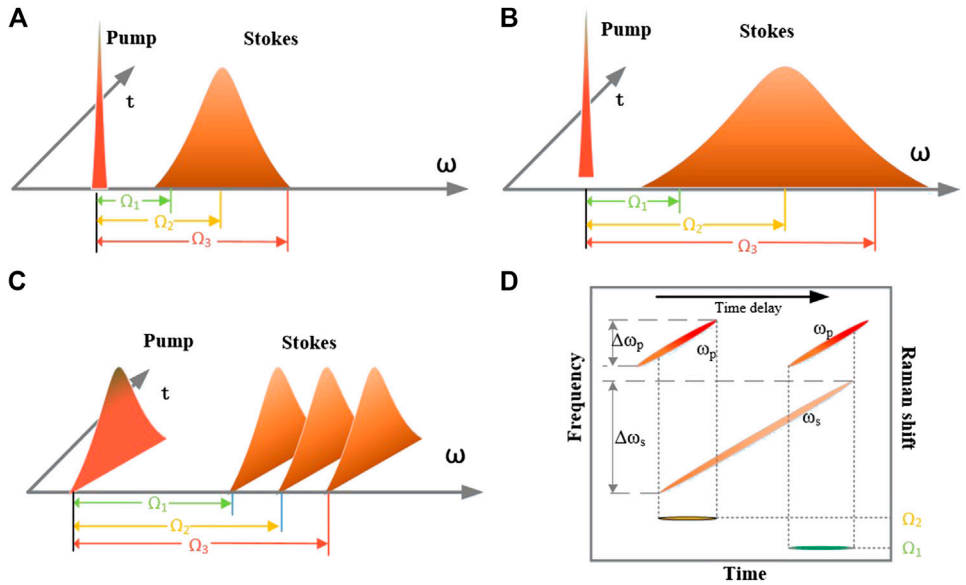

FIGURE 3 | Several common methods of multicolor CARS microscopy. **(A)** Picosecond pump and femtosecond Stokes pulses. **(B)** Picosecond pump and supercontinuum Stokes pulses. **(C)** Femtosecond pump and Stokes pulses with spectral focusing. **(D)** Principle of the spectral focusing method.

which can obtain a high spectral resolution when excited by a broadband light source. In this method, a dispersive medium is used to linearly chirp the light source. Although the linewidth of the chirped source remains the same, the instantaneous linewidth of the interaction between the two beams becomes very narrow. This instantaneous linewidth determines the spectral resolution of the system. The desired CARS spectrum can be obtained easily and quickly by adjusting the time delay between the pump and Stokes beams. In addition to being ingenious, this method has the advantage of being simple and fast. The disadvantages are the same as that of the ps-pump–fs-Stokes pulse method, i.e., it is not feasible to obtain a wide range of spectral signals simultaneously.

Over the past few years, it has become possible to study complex samples obtaining more detailed information for both biological and material science samples by multiplex CARS microscopy. Multiplex CARS microscopy confers the two key advantages of the full spectrum being available, and of being quantitative. The full spectrum is essential when studying complex samples with many overlapping peaks and the quantitative nature of the spectrum makes multiplex CARS microscopy a particularly useful technique for probing such complex samples. The extremely rich information obtained from imaging and spectral information constitutes a hyperspectral dataset. With the advent of phase retrieval techniques such as the maximum entropy method (MEM) and time-domain Kramers–Kronig (TD–KK) transformation, such spectra become amenable to analysis by multivariate techniques such as principal component analysis and related approaches. Therefore, the different components in the sample can be distinguished based on their vibrational information in an unlabeled manner, and the sensitivity of each component can be increased to the mM–μM level by using electronic resonance enhancement. Coupled with rapid spectral acquisition, these sophisticated algorithms should make it possible for researchers to investigate phenomena in the biological and material science fields that manifest as only subtle changes in the vibrational spectrum and occur on sub-micrometer length scales at sub-ms timescales.

APPLICATIONS OF CARS MICROSCOPY

Cell Imaging

CARS microscopy has been widely used for cell imaging [36, 45–53]. The strong CARS signal in the C-H stretching region can provide rich and unexpected chemical information, such as that related to lipids and proteins. For example, Nan et al. [54] used the CH_2 stretching vibration to map neutral lipid droplets in living fibroblasts. There was a significant process of disappearance of the lipid droplets in the cells in the early stage of differentiation, after which differentiation and accumulation began again. Paar et al. [55] used CARS microscopy to study the metabolism of intracellular lipid droplets during lipid decomposition. Experiments have shown that lipid droplet growth is achieved through the transfer of lipids between one organelle and another. This lipid transfer is not a rapid spontaneous process but completed within a few hours. Experimental data show that the growth of lipid droplets is a highly regulated process, and the decomposition and production of lipids occur in parallel in cells to prevent cell acid overflow. In another work [56], cancer cells *in vivo* and *in vitro* were monitored by CARS microscopy to assess the effect of diet on the metastasis of cancer cells. The results show that the physical disturbance of free fatty acids to the cancer cell membrane in lipid rich tumors is related to tumor metastasis. CARS has also been used to study prostate circulating carcinoma cells, and the results show that prostate circulatory carcinoma cells have a CARS signal

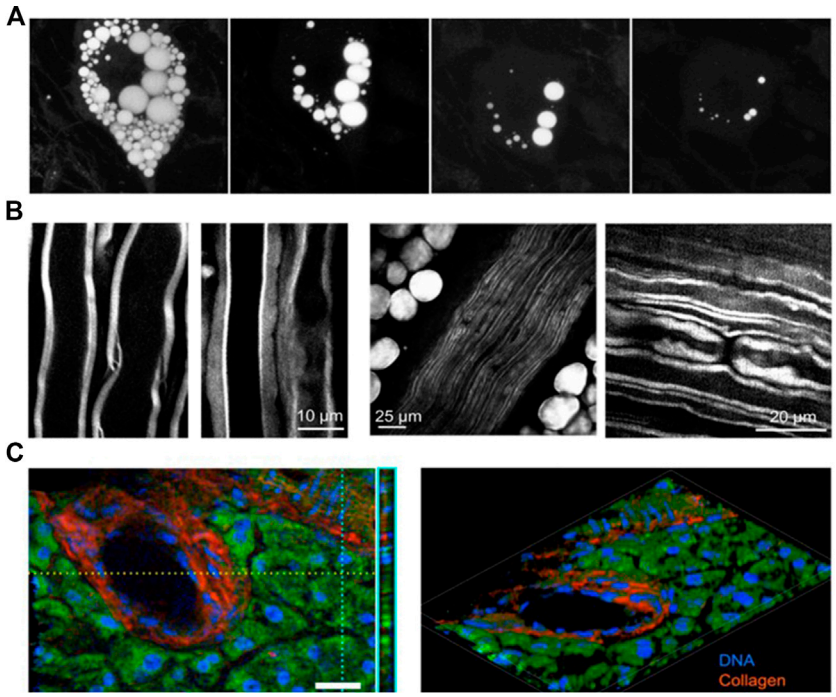

FIGURE 4 | (A) Adipocyte cellular lipid disintegration induced by forskolin [55]. **(B)** Imaging myelin sheath *ex vivo* and *in vivo* by CARS microscopy. **(C)** Extremely broadband, 785 cm^{-1} (nuclei) to 1,665 cm^{-1} (protein), CARS imaging of a murine pancreatic duct and 3D reconstruction imaging [60].

intensity seven times stronger than leukocytes [57]. The absorption and decomposition of surfactants in mammalian cells were studied by CARS spectroscopy [58]. The results show that living cells retain surfactants not only on the cell membrane but also throughout the intracellular membrane system. Label-free chemical mapping of cells by hyperspectral CARS microscopy has led to promising results. In another work, Di Napoli [59] fed different ratios of Palmitic acid and α-linolenic acid to human adipose derived stem cells and the results showed good contrast between cellular components and the corresponding CARS spectra.

Tissue Imaging

CARS has also been posited as a unique tool for label free tissue imaging. Visualization and characterization of the myelin sheath in the peripheral nervous system [61, 62] and central nervous system [63–67] is an important application. The sciatic nerve is a perfect candidate for *in vivo* CARS imaging since it is the largest single nerve in mammals and located in the peripheral nervous system isolated from the movement induced by breathing and the heartbeat. By 3D imaging of fat cells that surround the nerve, the underlying contrast mechanisms of *in vivo* CARS are found to arise from both interfaces and back reflection of the forward CARS signal [61]. Longitudinal *in vivo* CARS imaging of the spinal cord has been demonstrated through a careful experimental design to overcome complexities induced by laminectomy surgery [64]. To reduce the amount of tissue to be removed and improve the survivability and recovery time of the animals, the spine was exposed by making an incision through the skin and muscle tissue at T10, where the natural curvature of the spinal cord makes this region more superficial to the skin than at other locations [64]. The myelin sheath [63], myelinated axons [61], and the node of Ranvier [64] were distinguished clearly by CARS microscopy, as shown in **Figures 4B** left, middle, and right, respectively. The lipid metabolism in the atherosclerotic tissue of mouse and human subjects has been studied by CARS microscopy. Employing picosecond lasers, Wang et al. explored the imaging capabilities of CARS-based multimodal microscopy imaging of atherosclerosis. The study first demonstrated the capability to identify different atherosclerotic types [68] based on the scheme of atherosclerosis classification suggested by the American Heart Association (AHA) by imaging. Furthermore, Wang et al. [68] showed that a multimodal approach employing CARS and sum-frequency generation (SFG) signals allows quantitation of collagen and lipid content in lesions from early to advanced stages. Additional studies have shown increasing interest in using CARS microscopy for the studies of atherosclerotic lesions in animal models. Lim et al. utilized multimodal NLO microscopy to quantitatively measure the impact of a high-fat, high-cholesterol Western diet on the composition of atherosclerotic plaques in ApoE-deficient mice [69]. Using photonic crystal fiber-based CARS microscopy, the capability of multimodal imaging was demonstrated by an alternative femtosecond system to study lesion development in myocardial infarction-prone, hyperlipidemic rabbits [70]. Moreover, CARS has been used to skin biopsy [17, 71–74] and for stain-free histopathology. An imaging platform based on broadband coherent anti-Stokes Raman scattering (BCARS)

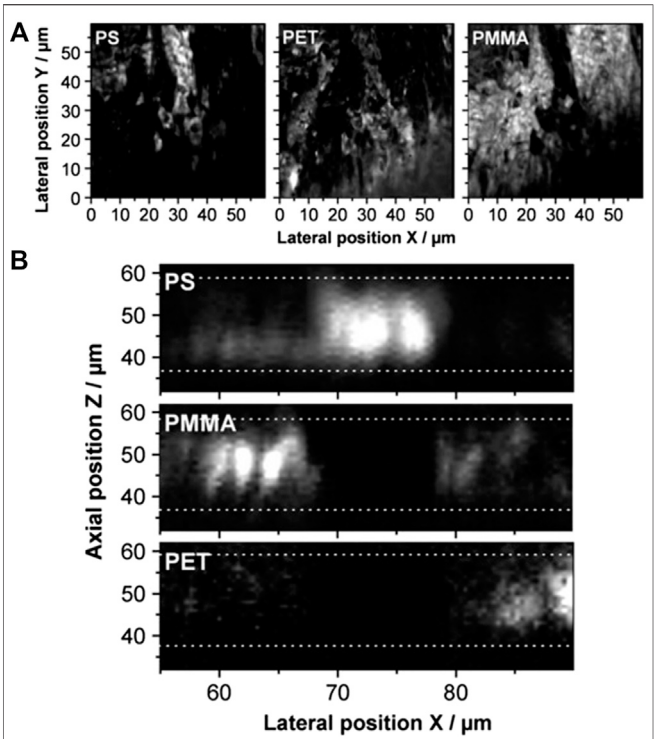

FIGURE 5 | CARS imaging of a polymer blend consisting of PS, PET, and PMMA. **(A)** Lateral and **(B)** axial views.

was developed by Camp et al. [60], and demonstrated 3D tissue imaging of a murine pancreatic duct showing the distributions of DNA, collagen, protein and lipids, as shown in **Figures 4C**. Recently, Wei-Wen [75] studied lipid particles in *Caenorhabditis elegans* by using this BCARS platform. The results show that fat particles in the adult intestine are diverse, and most are destined for the next generation. In comparison, fat particles in skin-like *epidermis* are similar and less dynamic.

Material Science

CARS microscopy lends itself well to the study of polymer films, thanks to the intrinsic sectioning capability of CARS and the intensity of the polymer peaks. Von Vacano et al. [35] were able to discriminate between the different polymers in tertiary blends of polystyrene (PS), polyethylene terephthalate (PET) and polymethylmethacrylate (PMMA), as well as to construct a virtual section of an adhesive and its carrier film, as shown in **Figure 5**. Jeoung group has also used the sectioning capability of multiplex CARS microscopy to quantitatively determine the thickness of sub-micron polymeric films [76, 77].

CARS microscopy has also been used to study reactions in zeolite crystals. CARS is an ideal tool to study the interplay between catalyst architecture and reactivity and hence obtain previously inaccessible information about fundamental processes of catalysts. Specifically, the precursor states of thiophene conversion over individual H-ZSM-5 zeolite crystals have been studied [78]. Maps of the catalyst loaded with thiophene revealed a heterogeneous, diffusion-limited distribution of thiophene throughout the zeolite, with the analytes accumulating at the center of the crystal and along defect sites.

More recently, Kotaro [79] developed a high-throughput flow cytometry system based on a Fourier-transform CARS spectrometer, enabling a high throughput of 2000 events/s. High chemical specificity and classification accuracy without labeling is demonstrated by the differentiation of polymer beads and *Euglena gracilis*. Super-resolution vibration imaging by higher-order CARS microscopy that detects higher-order anti-stokes Raman signals, such as six-wave mixing (SWM) at $\omega_{SWM} = 3\omega_p - 2\omega_S$ and eight-wave mixing (EWM) at $\omega_{EWM} = 4\omega_p - 3\omega_S$, increasing the respective lateral resolutions to 230 and 196 nm is reported by Li [80]. To increase the signal-to-noize radio and imaging speed, the wide-field CARS implementation was improved. Duarte [81] developed wide-field Fourier-transform coherent anti-Stokes Raman scattering microscopy with high-contrast, and outline detail of the wide-field FT-CARS signal. Heuke [82] implemented wide-field CARS by using a rotating disk with an imprinted modulation pattern and a PMT detector, referred to as spatial frequency modulated imaging (SPIFI). The results demonstrate that SPIFI-CARS could detect a much larger number of photons than that of laser-scanning microscopy (LSM)-CARS, and further, could be operated in ambient light.

OUTLOOK

Although the technological development of CARS is close to maturity, its application has just begun; however, the results are encouraging. Although CARS has broad application prospects, it will not replace other imaging methods in all fields. Because the cost of the spontaneous Raman system is relatively low and the system is relatively simple, it will likely be chosen when imaging speed is not a priority or there are technical difficulties (such as sample environment) to apply the coherent method. However, if the sample does not have second harmonic generation (SHG) characteristics, and fast acquisition is important, CARS or coherent Raman microscopy is the best label-free optical imaging method.

The clinical translation of CARS microscopy has long been hindered by traditional solid-state lasers that are sensitive to the environment. Ultrafast fiber lasers can potentially overcome these shortcomings but have not yet been fully exploited for CARS microscopy, as previous implementations have suffered from high intensity noise, a narrow tuning range, and low power, resulting in low image quality and slow imaging speed [23, 83–90]. Therefore, high-performance fiber lasers are highly required.

Another recent trend has been focusing on label-free multimodal nonlinear microscopy based on CARS, two-photon excited fluorescence (TPEF), and SHG [91–94]. The coupling of two-photon fluorescence, second-harmonic generation, and coherent anti-Stokes Raman scattering has allowed for investigation of a broad range of biological phenomena concerning lipid metabolism, cancer development, cardiovascular disease, and skin biology. By integrating the strengths of each non-linear optical (NLO) imaging modality, different structures and their interactions in a complex biological system can be simultaneously visualized.

Overall, as a label-free optical imaging method, CARS has a bright future with the development of other technologies such as laser light source and detection devices.

AUTHOR CONTRIBUTIONS

SL, LL and JQ wrote and edited the manuscript. SL, YL, RY, LL and JQ conceived the work and organized the manuscript.

FUNDING

This work was supported in part by National Natural Science Foundation of China (61525503/61620106016/61835009/61722508/61961136005/11904241), (Key) Project of Department of Education of Guangdong Province (2016KCXTD007), China Postdoctoral Science Foundation funded project (2018M643159) and Shenzhen Science and Technology Funding (JCYJ20180305124902165).

REFERENCES

1. Raman CV, Krishnan KS. A new type of secondary radiation. *Nature* (1928) 121(3048):501–2. doi:10.1038/121501c0
2. Cheng J-X, Volkmer A, Xie XS. Theoretical and experimental characterization of coherent anti-Stokes Raman scattering microscopy. *J Opt Soc Am B* (2002) 19(6):1363–75. doi:10.1364/josab.19.001363
3. Evans CL, Xie XS. Coherent anti-Stokes Raman scattering microscopy: chemical imaging for biology and medicine. *Annu Rev Anal Chem* (2008) 1:883–909. doi:10.1146/annurev.anchem.1.031207.112754
4. P Matousek M Morris, eds. *Emerging Raman applications and techniques in biomedical and pharmaceutical fields*. New York, NY: Springer Science & Business Media (2010)
5. Cheng JX, Xie XS. Vibrational spectroscopic imaging of living systems: an emerging platform for biology and medicine. *Science* (2015) 350(6264):aaa8870. doi:10.1126/science.aaa8870
6. Zhang C, Cheng J-X. Perspective: coherent Raman scattering microscopy, the future is bright. *APL Photonics* (2018) 3(9):090901. doi:10.1063/1.5040101
7. Rigneault H, Berto P. Tutorial: coherent Raman light matter interaction processes. *APL Photonics* (2018) 3(9):091101. doi:10.1063/1.5030335
8. Mazumder N, Balla NK, Zhuo GY, Kistenev YV, Kumar R, Kao FJ, et al. Label-free non-linear multimodal optical microscopy-basics, development, and applications. *Front Phys* (2019) 7:170. doi:10.3389/fphy.2019.00170
9. Terhune RW, Maker PD, Savage CM. Measurements of nonlinear light scattering. *Phys Rev Lett* (1965) 14(17):681–4. doi:10.1103/PhysRevLett.14.681
10. Begley RF, Harvey AB, Byer RL. Coherent anti-Stokes Raman spectroscopy. *Appl Phys Lett* (1974) 25(7):387–90
11. Duncan MD, Reintjes J, Manuccia TJ. Scanning coherent anti-Stokes Raman microscope. *Opt Lett* (1982) 7(8):350–2. doi:10.1364/ol.7.000350
12. Zumbusch A, Holtom GR, Xie XS. Three-dimensional vibrational imaging by coherent anti-Stokes Raman scattering. *Phys Rev Lett* (1999) 82(20):4142–5. doi:10.1103/PhysRevLett.82.4142
13. Djaker N, Lenne P-F, Marguet D, Colonna A, Hadjur C, Rigneault H. Coherent anti-Stokes Raman scattering microscopy (CARS): instrumentation and applications. *Nucl Instrum Methods Phys Res Sect A Accel Spectrom Detect Assoc Equip* (2007) 571(1-2):177–81. doi:10.1016/j.nima.2006.10.057
14. Cheng J-X. Coherent anti-Stokes Raman scattering microscopy. *Appl Spectrosc* (2007) 61(9):197–208. doi:10.1366/000370207781746044
15. Cheng J-X, Xie XS. Coherent anti-Stokes Raman scattering microscopy: instrumentation, theory, and applications. *J Phys Chem B* (2004) 108(3):827–40. doi:10.1021/jp035693v
16. Cheng JX, Jia YK, Zheng G, Xie XS. Laser-scanning coherent anti-Stokes Raman scattering microscopy and applications to cell biology. *Biophys J* (2002) 83(1):502–9. doi:10.1016/S0006-3495(02)75186-2
17. Evans CL, Potma EO, Puoris'haag M, Côté D, Lin CP, Xie XS. Chemical imaging of tissue *in vivo* with video-rate coherent anti-Stokes Raman scattering microscopy. *Proc Natl Acad Sci USA* (2005) 102(46):16807–12. doi:10.1073/pnas.0508282102
18. Ganikhanov F, Evans CL, Saar BG, Xie XS. High-sensitivity vibrational imaging with frequency modulation coherent anti-Stokes Raman scattering (FM CARS) microscopy. *Opt Lett* (2006) 31(12):1872–4. doi:10.1364/ol.31.001872
19. Marks DL, Boppart SA. Nonlinear interferometric vibrational imaging. *Phys Rev Lett* (2004) 92(12):123905. doi:10.1103/PhysRevLett.92.123905
20. Liu Y, Lee YJ, Cicerone MT. Broadband CARS spectral phase retrieval using a time-domain Kramers-Kronig transform. *Opt Lett* (2009) 34(9):1363–5. doi:10.1364/OL.34.001363
21. Ganikhanov F, Carrasco S, Sunney Xie X, Katz M, Seitz W, Kopf D. Broadly tunable dual-wavelength light source for coherent anti-Stokes Raman scattering microscopy. *Opt Lett* (2006) 31(9):1292–4. doi:10.1364/OL.31.001292
22. Murugkar S, Brideau C, Ridsdale A, Naji M, Stys PK, Anis H. Coherent anti-Stokes Raman scattering microscopy using photonic crystal fiber with two closely lying zero dispersion wavelengths. *Optic Express* (2007) 15(21):14028–37. doi:10.1364/OE.15.014028
23. Kieu K, Saar BG, Holtom GR, Xie XS, Wise FW. High-power picosecond fiber source for coherent Raman microscopy. *Opt Lett* (2009) 34(13):2051–3. doi:10.1364/ol.34.002051
24. Cheng J-X, Volkmer A, Book LD, Xie XS. An epi-detected coherent anti-Stokes Raman scattering (E-CARS) microscope with high spectral resolution and high sensitivity. *J Phys Chem B* (2001) 105(7):1277–80. doi:10.1021/jp003774a
25. Pegoraro AF, Ridsdale A, Moffatt DJ, Jia Y, Pezacki JP, Stolow A. Optimally chirped multimodal CARS microscopy based on a single Ti:sapphire oscillator. *Optic Express* (2009) 17(4):2984–96. doi:10.1364/OE.17.002984
26. Chen H, Wang H, Slipchenko MN, Jung Y, Shi Y, Zhu J, et al. A multimodal platform for nonlinear optical microscopy and microspectroscopy. *Optic Express* (2009) 17(3):1282–90. doi:10.1364/OE.17.001282
27. Ozeki Y, Dake F, Kajiyama S, Fukui K, Itoh K. Analysis and experimental assessment of the sensitivity of stimulated Raman scattering microscopy. *Optic Express* (2009) 17(5):3651–8. doi:10.1364/OE.17.003651
28. Cheng J-X, Volkmer A, Book LD, Xie XS. Multiplex coherent anti-Stokes Raman scattering microspectroscopy and study of lipid vesicles. *J Phys Chem B* (2002) 106(34):8493–8. doi:10.1021/jp025771z
29 Müller M, Schins JM. Imaging the thermodynamic state of lipid membranes with multiplex CARS microscopy. *J Phys Chem B* (2002) 106(14):3715–23. doi:10.1021/jp014012y
30. Chen BC, Sung J, Wu X, Lim SH. Chemical imaging and microspectroscopy with spectral focusing coherent anti-Stokes Raman scattering. *J Biomed Optic* (2011) 16(2):021112. doi:10.1117/1.3533315
31. Hashimoto K, Omachi J, Ideguchi T. Ultra-broadband rapid-scan Fourier-transform CARS spectroscopy with sub-10-fs optical pulses. *Optic Express* (2018) 26(11):14307–14. doi:10.1364/OE.26.014307
32. Kano H, Hamaguchi H-O. Ultrabroadband (> 2500 cm^{-1}) multiplex coherent anti-Stokes Raman scattering microspectroscopy using a supercontinuum generated from a photonic crystal fiber. *Appl Phys Lett* (2005) 86(12):121113. doi:10.1063/1.1883714
33. Kee TW, Cicerone MT. Simple approach to one-laser, broadband coherent anti-Stokes Raman scattering microscopy. *Opt Lett* (2004) 29(23):2701–3. doi:10.1364/ol.29.002701
34. Parekh SH, Lee YJ, Aamer KA, Cicerone MT. Label-free cellular imaging by broadband coherent anti-Stokes Raman scattering microscopy. *Biophys J* (2010) 99(8):2695–704. doi:10.1016/j.bpj.2010.08.009
35. von Vacano B, Meyer L, Motzkus M. Rapid polymer blend imaging with quantitative broadband multiplex CARS microscopy. *J Raman Spectrosc* (2007) 38(7):916–26. doi:10.1002/jrs.1704
36. Okuno M, Kano H, Leproux P, Couderc V, Day JP, Bonn M, et al. Quantitative CARS molecular fingerprinting of single living cells with the use of the maximum entropy method. *Angew Chem Int Ed Engl* (2010) 49(38):6773–7. doi:10.1002/anie.201001560

37. Okuno M, Kano H, Leproux P, Couderc V, Hamaguchi HO. Ultrabroadband multiplex CARS microspectroscopy and imaging using a subnanosecond supercontinuum light source in the deep near infrared. *Opt Lett* (2008) 33(9):923–5. doi:10.1364/ol.33.000923
38. Hellerer T, Annika MK, Zumbusch A. Spectral focusing: high spectral resolution spectroscopy with broad-bandwidth laser pulses. *Appl Phys Lett* (2004) 85(1):25–7. doi:10.1063/1.1768312
39. Rocha-Mendoza I, Langbein W, Borri P. Coherent anti-Stokes Raman microspectroscopy using spectral focusing with glass dispersion. *Appl Phys Lett* (2008) 93(20):201103. doi:10.1063/1.3028346
40. Langbein W, Rocha-Mendoza I, Borri P. Coherent anti-Stokes Raman microspectroscopy using spectral focusing: theory and experiment. *J Raman Spectrosc* (2009) 40(7):800–8. doi:10.1002/jrs.2264
41. Langbein W, Rocha-Mendoza I, Borri P. Single source coherent anti-Stokes Raman microspectroscopy using spectral focusing. *Appl Phys Lett* (2009) 95(8):081109. doi:10.1063/1.3216073
42. Gu M, Satija A, Lucht RP. Impact of moderate pump–Stokes chirp on femtosecond coherent anti-Stokes Raman scattering spectra. *J Raman Spectrosc* (2020) 51(1):115–24. doi:10.1002/jrs.5754
43. Fu D, Holtom G, Freudiger C, Zhang X, Xie XS. Hyperspectral imaging with stimulated Raman scattering by chirped femtosecond lasers. *J Phys Chem B* (2013) 117(16):4634–40. doi:10.1021/jp308938t
44. Rocha-Mendoza I, Langbein W, Watson P, Borri P. Differential coherent anti-Stokes Raman scattering microscopy with linearly chirped femtosecond laser pulses. *Opt Lett* (2009) 34(15):2258–60. doi:10.1364/ol.34.002258
45. Segawa H, Okuno M, Kano H, Leproux P, Couderc V, Hamaguchi HO. Label-free tetra-modal molecular imaging of living cells with CARS, SHG, THG and TSFG (coherent anti-Stokes Raman scattering, second harmonic generation, third harmonic generation and third-order sum frequency generation). *Optic Express* (2012) 20(9):9551–7. doi:10.1364/OE.20.009551
46. Kano H. Molecular spectroscopic imaging using a white-light laser source. *Bull Chem Soc Jpn* (2010) 83(7):735–43. doi:10.1246/bcsj.20100004
47. Chen BC, Sung J, Lim SH. Chemical imaging with frequency modulation coherent anti-Stokes Raman scattering microscopy at the vibrational fingerprint region. *J Phys Chem B* (2010) 114(50):16871–80. doi:10.1021/jp104553s
48. Brackmann C, Norbeck J, Åkeson M, Bosch D, Larsson C, Gustafsson L, et al. CARS microscopy of lipid stores in yeast: the impact of nutritional state and genetic background. *J Raman Spectrsc* (2009) 40(7):748–56. doi:10.1002/jrs.2356
49. Vartiainen EM, Rinia HA, Müller M, Bonn M. Direct extraction of Raman line-shapes from congested CARS spectra. *Optic Express* (2006) 14(8):3622–30. doi:10.1364/OE.14.003622
50. Shimada R, Kano H, Hamaguchi HO. Hyper-Raman microspectroscopy: a new approach to completing vibrational spectral and imaging information under a microscope. *Opt Lett* (2006) 31(3):320–2. doi:10.1364/OL.31.000320
51. Ivleva NP, Niessner R, Panne U. Characterization and discrimination of pollen by Raman microscopy. *Anal Bioanal Chem* (2005) 381(1):261–7. doi:10.1007/s00216-004-2942-1
52. van Manen H-J, Kraan YM, Roos D, Otto C. Intracellular chemical imaging of heme-containing enzymes involved in innate immunity using resonance Raman microscopy. *J Phys Chem B* (2004) 108(48):18762–71. doi:10.1021/jp046955b
53. McConnell G, Riis E. Photonic crystal fibre enables short-wavelength two-photon laser scanning fluorescence microscopy with fura-2. *Phys Med Biol* (2004) 49(20):4757. doi:10.1088/0031-9155/49/20/007
54. Nan X, Cheng JX, Xie XS. Vibrational imaging of lipid droplets in live fibroblast cells with coherent anti-Stokes Raman scattering microscopy. *J Lipid Res* (2003) 44(11):2202–8. doi:10.1194/jlr.D300022-JLR200
55. Paar M, Jüngst C, Steiner NA, Magnes C, Sinner F, Kolb D, et al. Remodeling of lipid droplets during lipolysis and growth in adipocytes. *J Biol Chem* (2012) 287(14):11164–73. doi:10.1074/jbc.M111.316794
56. Le TT, Huff TB, Cheng JX. Coherent anti-Stokes Raman scattering imaging of lipids in cancer metastasis. *BMC Canc* (2009) 9(1):42. doi:10.1186/1471-2407-9-42
57. Mitra R, Chao O, Urasaki Y, Goodman OB, Le TT. Detection of lipid-rich prostate circulating tumour cells with coherent anti-Stokes Raman scattering microscopy. *BMC Canc* (2012) 12(1):540. doi:10.1186/1471-2407-12-540
58. Okuno M, Kano H, Fujii K, Bito K, Naito S, Leproux P, et al. Surfactant uptake dynamics in mammalian cells elucidated with quantitative coherent anti-Stokes Raman scattering microspectroscopy. *PloS One* (2014) 9(4):e93401. doi:10.1371/journal.pone.0093401
59. Di Napoli C, Pope I, Masia F, Watson P, Langbein W, Borri P. Hyperspectral and differential CARS microscopy for quantitative chemical imaging in human adipocytes. *Biomed Optic Express* (2014) 5(5):1378–90. doi:10.1364/BOE.5.001378
60. Camp CH, Jr, Lee YJ, Heddleston JM, Hartshorn CM, Hight Walker AR, Rich JN, et al. High-speed coherent Raman fingerprint imaging of biological tissues. *Nat Photon* (2014) 8(8):627–34. doi:10.1038/nphoton.2014.145
61. Huff TB, Cheng JX. *In vivo* coherent anti-Stokes Raman scattering imaging of sciatic nerve tissue. *J Microsc* (2007) 225(2):175–82. doi:10.1111/j.1365-2818.2007.01729.x
62. Jung Y, Ng JH, Keating CP, Senthil-Kumar P, Zhao J, Randolph MA, et al. Comprehensive evaluation of peripheral nerve regeneration in the acute healing phase using tissue clearing and optical microscopy in a rodent model. *PloS One* (2014) 9(4):e94054. doi:10.1371/journal.pone.0094054
63. Fu Y, Wang H, Huff TB, Shi R, Cheng JX. Coherent anti-Stokes Raman scattering imaging of myelin degradation reveals a calcium-dependent pathway in lyso-PtdCho-induced demyelination. *J Neurosci Res* (2007) 85(13):2870–81. doi:10.1002/jnr.21403
64. Shi Y, Zhang D, Huff TB, Wang X, Shi R, Xu XM, et al. Longitudinal *in vivo* coherent anti-Stokes Raman scattering imaging of demyelination and remyelination in injured spinal cord. *J Biomed Optic* (2011) 16(10):106012. doi:10.1117/1.3641988
65. Bélanger E, Henry FP, Vallée R, Randolph MA, Kochevar IE, Winograd JM, et al. *In vivo* evaluation of demyelination and remyelination in a nerve crush injury model. *Biomed Optic Express* (2011) 2(9):2698–708. doi:10.1364/BOE.2.002698
66. Shi Y, Kim S, Huff TB, Borgens RB, Park K, Shi R, et al. Effective repair of traumatically injured spinal cord by nanoscale block copolymer micelles. *Nat Nanotechnol* (2010) 5(1):80–7. doi:10.1038/nnano.2009.303
67. Wang H, Fu Y, Zickmund P, Shi R, Cheng JX. Coherent anti-Stokes Raman scattering imaging of axonal myelin in live spinal tissues. *Biophys J* (2005) 89(1):581–91. doi:10.1529/biophysj.105.061911
68. Wang HW, Langohr IM, Sturek M, Cheng JX. Imaging and quantitative analysis of atherosclerotic lesions by CARS-based multimodal nonlinear optical microscopy. *Arterioscler Thromb Vasc Biol* (2009) 29(9):1342–8. doi:10.1161/ATVBAHA.109.189316
69. Lim RS, Suhalim JL, Miyazaki-Anzai S, Miyazaki M, Levi M, Potma EO, et al. Identification of cholesterol crystals in plaques of atherosclerotic mice using hyperspectral CARS imaging. *J Lipid Res* (2011) 52(12):2177–86. doi:10.1194/jlr.M018077
70. Mostaço-Guidolin LB, Sowa MG, Ridsdale A, Pegoraro AF, Smith MS, Hewko MD, et al. Differentiating atherosclerotic plaque burden in arterial tissues using femtosecond cars-based multimodal nonlinear optical imaging. *Biomed Optic Express* (2010) 1(1):59–73. doi:10.1364/BOE.1.000059
71. Kiss N, Krolopp Á, Lőrincz K, Bánvölgyi A, Szipőcs R, Wikonkál N. Stain-free histopathology of basal cell carcinoma by dual vibration resonance frequency cars microscopy. *Pathol Oncol Res* (2018) 24(4):927–30. doi:10.1007/s12253-017-0356-6
72. Breunig HG, Bückle R, Kellner-Höfer M, Weinigel M, Lademann J, Sterry W, et al. Combined *in Vivo* multiphoton and cars imaging of healthy and disease-affected human skin. *Microsc Res Tech* (2012) 75(4):492–8. doi:10.1002/jemt.21082
73. König K, Breunig HG, Bückle R, Kellner-Höfer M, Weinigel M, Büttner E, et al. Optical skin biopsies by clinical CARS and multiphoton fluorescence/SHG tomography. *Laser Phys Lett* (2011) 8(6):465. doi:10.1002/lapl.201110014
74. Vogler N, Meyer T, Akimov D, Latka I, Krafft C, Bendsoe N, et al. Multimodal imaging to study the morphochemistry of basal cell carcinoma. *J Biophot* (2010) 3(10-11):728–36. doi:10.1002/jbio.201000071
75. Chen W-W, Lemieux GA, Camp CH, Chang T-C, Ashrafi K, Cicerone MT. Spectroscopic coherent Raman imaging of *Caenorhabditis elegans* reveals lipid particle diversity. *Nat Chem Biol* (2020) 16:1087–95. doi:10.1038/s41589-020-0565-2
76. Choi DS, Jeoung SC, Chon BH. Thickness dependent CARS measurement of polymeric thin films without depth-profiling. *Optic Express* (2008) 16(4):2604–13. doi:10.1364/oe.16.002604

77. Yahng JS, Jeoung SC. Thickness determination with chemical identification of double-layered polymeric thin film by using multiplex CARS. *Optic Laser Eng* (2011) 49(1):66–70. doi:10.1016/j.optlaseng.2010.08.016
78. Kox MH, Domke KF, Day JP, Rago G, Stavitski E, Bonn M, et al. Label-free chemical imaging of catalytic solids by coherent anti-Stokes Raman scattering and synchrotron-based infrared microscopy. *Angew Chem Int Ed Engl* (2009) 48(47):8990–4. doi:10.1002/anie.200904282
79. Hiramatsu K, Ideguchi T, Yonamine Y, Lee S, Luo Y, Hashimoto K, et al. High-throughput label-free molecular fingerprinting flow cytometry. *Sci Adv* (2019) 5(1):eaau0241. doi:10.1126/sciadv.aau0241
80. Gong L, Zheng W, Ma Y, Huang Z. Higher-order coherent anti-Stokes Raman scattering microscopy realizes label-free super-resolution vibrational imaging. *Nat Photon* (2019) 14:115–22. doi:10.1038/s41566-019-0535-y
81. Duarte AS, Schnedermann C, Kukura P. Wide-field detected fourier transform CARS microscopy. *Sci Rep* (2016) 6:37516. doi:10.1038/srep37516
82. Heuke S, Sivankutty S, Scotte C, Stockton P, Bartels RA, Sentenac A, et al. Spatial frequency modulated imaging in coherent anti-Stokes Raman microscopy. *Optica* (2020) 7(5):417–24. doi:10.1364/Optica.386526
83. Kong C, Pilger C, Hachmeister H, Wei X, Cheung TH, Lai CSW, et al. High-contrast, fast chemical imaging by coherent Raman scattering using a self-synchronized two-colour fibre laser. *Light Sci Appl* (2020) 9(1):25. doi:10.1038/s41377-020-0259-2
84. Tai B. *Fiber-based high energy ultrafast sources for nonlinear microscopy*. [PhD thesis]. Ann Arbor (MI): Boston University (2019).
85. Xu C, Wise FW. Recent advances in fiber lasers for nonlinear microscopy. *Nat Photon* (2013) 7(11):875–82. doi:10.1038/nphoton.2013.284
86. Baumgartl M, Gottschall T, Abreu-Afonso J, Díez A, Meyer T, Dietzek B, et al. Alignment-free, all-spliced fiber laser source for CARS microscopy based on four-wave-mixing. *Optic Express* (2012) 20(19):21010–8. doi:10.1364/OE.20.021010
87. Wang K, Freudiger CW, Lee JH, Saar BG, Xie XS, Xu C. All fiber, 1064-nm time-lens source for coherent anti-Stokes Raman scattering and stimulated Raman scattering microscopy. *Proc SPIE* (2011) Xi7903:79030. doi:10.1117/12.875898
88. Selm R, Winterhalder M, Zumbusch A, Krauss G, Hanke T, Sell A, et al. Ultrabroadband background-free coherent anti-Stokes Raman scattering microscopy based on a compact Er:fiber laser system. *Opt Lett* (2010) 35(19):3282–4. doi:10.1364/OL.35.003282
89. Pegoraro AF, Ridsdale A, Moffatt DJ, Pezacki JP, Thomas BK, Fu L, et al. All-fiber CARS microscopy of live cells. *Optic Express* (2009) 17(23):20700–6. doi:10.1364/OE.17.020700
90. Andresen ER, Nielsen CK, Thøgersen J, Keiding SR. Fiber laser-based light source for coherent anti-Stokes Raman scattering microspectroscopy. *Optic Express* (2007) 15(8):4848–56. doi:10.1364/oe.15.004848
91. Yarbakht M, Pradhan P, Köse-Vogel N, Bae H, Stengel S, Meyer T, et al. Nonlinear multimodal imaging characteristics of early septic liver injury in a mouse model of peritonitis. *Anal Chem* (2019) 91(17):11116–21. doi:10.1021/acs.analchem.9b01746
92. Meyer T, Bae H, Hasse S, Winter J, Woedtke TV, Schmitt M, et al. Multimodal nonlinear microscopy for therapy monitoring of cold atmospheric plasma treatment. *Micromachines* (2019) 10(9). doi:10.3390/mi10090564
93. Li R, Wang X, Zhou Y, Zong H, Chen M, Sun M. Advances in nonlinear optical microscopy for biophotonics. *J Nanophotonics* (2018) 12(3):033007. doi:10.1117/1.JNP.12.033007
94. Pegoraro AF, Slepkov AD, Ridsdale A, Moffatt DJ, Stolow A. Hyperspectral multimodal CARS microscopy in the fingerprint region. *J Biophot* (2014) 7(1-2):49–58. doi:10.1002/jbio.201200171

Conflict of Interest: The authors declare that the research was conducted in the absence of any commercial or financial relationships that could be construed as a potential conflict of interest.